Contrib Mineral Petrol (1999) 137: 102–114

Max Wilke · Harald Behrens

The dependence of the partitioning of iron and europium between plagioclase and hydrous tonalitic melt on oxygen fugacity

Received: 14 October 1998 / Received: 5 March 1999

Abstract The dependence of iron and europium partitioning between plagioclase and melt on oxygen fugacity was studied in the system SiO_2(Qz)—$NaAlSi_3O_8$(Ab)—$CaAl_2Si_2O_8$(An)—H_2O. Experiments were performed at 500 MPa and 850 °C/750 °C under water saturated conditions. The oxygen fugacity was varied in the log f_{O_2}-range from −7.27 to −15.78. To work at the most reducing conditions the classical double-capsule technique was modified. The sample and a C—O—H bearing sensor capsule were placed next to each other within a BN jacket to minimise loss of hydrogen to the vessel atmosphere. By this setup redox conditions slightly more reducing than the FeO—Fe_3O_4 buffer could be maintained even in 96 h runs. Raman spectra showed that the BN was modified by reaction with hydrogen resulting in a low hydrogen permeability. The partition coefficients determined for Eu at 850 °C and 500 MPa vary from 0.095 at conditions of the Cu—Cu_2O buffer to 1.81 at the most reducing conditions (C—O—H sensor). In the same f_{O_2} interval the partition coefficient for Fe varies from 0.55 at oxidising conditions to 0.08 at the most reducing conditions. The partitioning of Sm, which was added as a reference for a trivalent REE, does not vary with the oxygen fugacity, yielding an average value for $D = 0.07$. Lowering the temperature to 750 °C for a given f_{O_2} decreases the partition coefficient of Eu and increases that of Fe. Comparison with published data at 1 atm and at higher temperatures shows that both temperature and composition of the melt have strong effects on the partitioning behaviour. As the change of the partition coefficients in the geologically relevant f_{O_2} range is quite strong, element partitioning of Eu and Fe might be used to estimate redox conditions for the genesis of igneous rocks. Furthermore, by modelling the partitioning data it is possible to extract information about the redox state of the melt. Resulting ferric-ferrous ratios show significant differences from those predicted by empirical models.

M. Wilke (✉) · H. Behrens
Institut für Mineralogie, Universität Hannover,
Welfengarten 1, D-30167 Hannover, Germany
Tel.: +49-511-7624818, Fax: +49-511-7623045;
e-mail: max.wilke@mineralogie.uni-hannover.de

Editorial responsibility: J. Hoefs

Introduction

The redox conditions during the formation of igneous rocks can have a strong effect on the resulting phase assemblages (Scaillet 1995; Rutherford and Devine 1996; Martel et al. 1998). Hence there is a need to quantify the oxygen fugacity prevailing during the genesis of these rocks. Most of the changes in phase assemblages are due to the changing redox state of heterovalent elements like Fe and Eu. The partitioning of these elements between coexisting phases is strongly dependent on the oxygen fugacity. If pressure and temperature are known, the redox conditions during the formation of igneous rocks can be quantified using well calibrated redox sensors, e.g. coexisting iron-titanium oxides (Spencer and Lindsley 1981; Andersen and Lindsley 1988). Estimates by this sensor at rather oxidising conditions (NNO + 1.3), however, must be treated with caution since extra components in ilmenite expand the solvus in a way that is not accommodated for in the current model of the thermobarometer (Lindsley and Frost 1992; Evans and Scaillet 1997).

However, numerous igneous rocks do not contain ilmenite and thus this thermobarometer cannot be applied. Another approach is to bracket the redox conditions during the formation of igneous rocks by using the partitioning of iron and europium between plagioclase and melt. Both elements have two stable oxidation states, M^{2+} and M^{3+} and thus their partitioning behaviour is dependent on the oxygen fugacity. Different incorporation schemes in plagioclase are observed for M^{2+} and M^{3+}.

In the case of Eu, two substitution mechanisms have been verified experimentally: (i) $Eu^{2+} \leftrightarrow Ca^{2+}$ and (ii) $3\ Ca^{2+} \leftrightarrow 2\ Eu^{3+} + V$ where V denotes a vacancy (Kimata 1988). Incorporation of a trivalent cation on the Ca site of plagioclase is rather unfavourable and the first substitution scheme is strongly preferred. This also is supported by the Eu anomaly found in igneous rocks with residual plagioclase. In contrast to the other rare earth elements (REE), Eu also exists in the divalent state under geological conditions leading to enrichment of Eu in plagioclase.

Incorporation of Fe into the feldspar structure is more complex and at least three substitution mechanisms can occur: (i) $Fe^{3+} \leftrightarrow Al^{3+}$, (ii) $Fe^{2+} \leftrightarrow Ca^{2+}$, (iii) $Fe^{2+} + Si^{4+} \leftrightarrow 2\ Al^{3+}$. In alkali feldspars only the first substitution scheme has been observed (Coombs 1954; Hofmeister and Rossman 1984). Plagioclase can also incorporate Fe^{2+} and there is experimental evidence for substitution schemes (ii) and (iii) (Longhi et al. 1976; Hofmeister and Rossman 1984, Behrens et al. 1990). Hofmeister and Rossman (1984) have found by spectroscopic investigation of terrestrial plagioclase a positive correlation of the Fe^{2+}/Fe^{3+} to the An content of the plagioclase with Fe^{2+} becoming dominant only in pure anorthite.

Several attempts have been made to elucidate the oxygen fugacity dependence for the partitioning of europium (Drake 1975; Weill and McKay 1975) and iron (Phinney 1992; Sato 1989) between basaltic melts and plagioclase. All experiments were performed at 1 atm and temperatures around 1200 °C. These studies have shown a variation of the partition coefficients ($D = c_{crystal}/c_{melt}$, c in weight percent) of about 1.5 log units for Eu and of about 0.6 log units for Fe in the log f_{O_2}-range −6 to 0.7.

As natural magmas often contain water it is important to know the influence of water dissolved in the melt on the partitioning. Furthermore, the effect of anhydrous melt composition is not known. Extrapolation of the data obtained for basaltic melts at high temperature to granitic and tonalitic melts at lower temperatures is highly uncertain. In this paper we present data on the partitioning of Eu and Fe between melt and plagioclase in the haplotonalitic system SiO_2(Qz)—$NaAlSi_3O_8$(Ab)—$CaAl_2Si_2O_8$(An)—H_2O at 500 MPa pressure and 850 °C/750 °C at water saturation. A central part of this paper is the presentation of the technical improvements we have applied to the solid-buffer technique to maintain highly reducing conditions in internally heated pressure vessels (IHPV) at high temperatures. Furthermore, we give a model to describe the f_{O_2}-dependence of the element partitioning and show how information about the redox state of the melt can be extracted from the partitioning data.

Experimental techniques

Starting materials and experimental apparatus

The experiments were performed in the system SiO_2(Qz)—$NaAlSi_3O_8$(Ab)—$CaAl_2Si_2O_8$(An)—H_2O. A plagioclase-rich composition was chosen for the 850 °C experiments and a silica-rich composition for the 750 °C experiments so that high melt/plagioclase ratios were obtained for both temperatures. The synthetic glasses contained 0.5 wt% Eu_2O_3 and Sm_2O_3. As Sm does not change its redox state it is a reference for the partitioning of a trivalent REE. In experiments at 750 °C (500 MPa) using glasses doped with Sm and Eu, many tiny needles of a REE-rich phase were formed and no crystal-free area in the glass could be found sufficiently large to perform microprobe analyses. Hence the experiments at 750 °C had to be done with Eu only. Glasses for Fe partitioning experiments were doped with 1.5 wt% Fe_2O_3. In order to establish identical run conditions it would have been preferable to use Fe, Eu and Sm in the same experiment, but doping the glasses with both REE and Fe lead to precipitation of allanite. Therefore, Fe and Eu partitioning have to be studied separately. The anhydrous glasses were synthesised from oxides and carbonates at 1600 °C in platinum crucibles and checked by electron microprobe for homogeneity. The compositions of the anhydrous starting glasses are shown in Table 1.

Disequilibrium growth of plagioclase was observed in runs using anhydrous or water poor glass as starting material. We attribute this to the rather slow diffusion of the water (Behrens and Nowak 1997; Nowak and Behrens 1997) into the initially anhydrous glass and to slow relaxation of the highly viscous melt (Schulze et al. 1996). Therefore glasses containing about 10 wt% H_2O which were pre-saturated at the same pressure but at higher temperature, were used as starting material. To synthesise the Eu-bearing glasses the crushed anhydrous glass was sealed together with 12 wt% H_2O in Pt capsules and annealed at 1200 °C and 500 MPa for 48 h. In order to minimise iron loss to the capsule glasses containing Fe were synthesised at lower temperature (1000 °C) in shorter runs (30 h) using Au capsules. The water contents of the glasses were analysed by Karl-Fischer Titration (Behrens 1995). In the partitioning experiments single pieces of the hydrous glasses were enclosed in Pt capsules together with an appropriate amount of water to ensure saturated conditions. For Fe bearing glasses Ag capsules were used except for runs using the Cu—Cu_2O buffer because alloying of Cu and Ag lead to melting of the capsules. Pt was used for these runs as dissolution of Fe in Pt is small at such oxidising conditions. To encourage growth of few but rather big plagioclase crystals all samples were annealed for 30 min at conditions above the liquidus and then cooled at 1–0.5 °C/min to the run temperature (retrograde temperature path).

Table 1 Electron microprobe analyses and CIPW normative compositions of anhydrous starting glasses. All data given in wt%

	To1(Eu)	To2(Eu)	To1(Fe)	To2(Fe)
SiO_2	70.18	76.77	70.57	76.08
Al_2O_3	19.03	15.05	17.85	14.49
CaO	7.35	6.65	7.32	6.00
Na_2O	3.46	2.10	3.41	2.56
Fe_2O_3	–	–	1.57	1.58
Eu_2O_3	0.51	0.47	–	–
Sm_2O_3	0.52	–	–	–
Total	101.05	101.04	100.89	100.71
Qz	34.3	49.8	35.0	48.5
Ab	29.2	17.6	28.8	21.7
An	36.5	32.6	36.2	29.8
C	0.0	0.0	0.0	0.0

The experiments were performed in two different types of pressure vessels: (1) horizontally orientated cold-seal pressure vessels (CSPV) pressurised with water, and (2) vertically orientated internally heated pressure vessels (IHPV) pressurised with argon.

Type (1): The CSPV used for experiments at 750 °C are made of a superalloy (Vakumelt 2.4888) with an inner diameter of 6 mm. To minimise temperature gradients the free volume was filled by inconel filler rods. The temperature was controlled by an external, sheathed type-K thermocouple. The temperature at the sample position was calibrated to the external thermocouple using a calibration vessel. The recorded temperature is believed to be accurate within ±8 °C. Pressure was measured with a strain gauge manometer with an uncertainty of ±50 bar (for details on the CSPV see Puziewicz and Johannes 1988). A temperature of 700 °C was reached after 18 min and 750 °C after 30 min. Samples were quenched isobarically in a flux of compressed air resulting in an initial quench rate of 250 °C/min.

Type (2): The IHPV used for all experiments above 800 °C has a working volume of 15 mm in diameter and 50 mm in length within the hot spot zone. Pressure was measured with a strain gauge manometer with an uncertainty of ±50 bar. The temperature in the hot spot zone was monitored using three sheathed type-K thermocouples spaced 20 mm apart. The IHPV was heated by a two-loop furnace made of molybdenum wire. The temperature variation in the whole working volume was below ±10 °C in all experiments. The samples were heated to superliquidus temperature at a constant rate of 30 °C/min using a programmable controller (Eurotherm 900 Series). The samples were quenched at an average rate of 150 °C/min to below 400 °C. Constant pressure was maintained during cooling by automatic pumping.

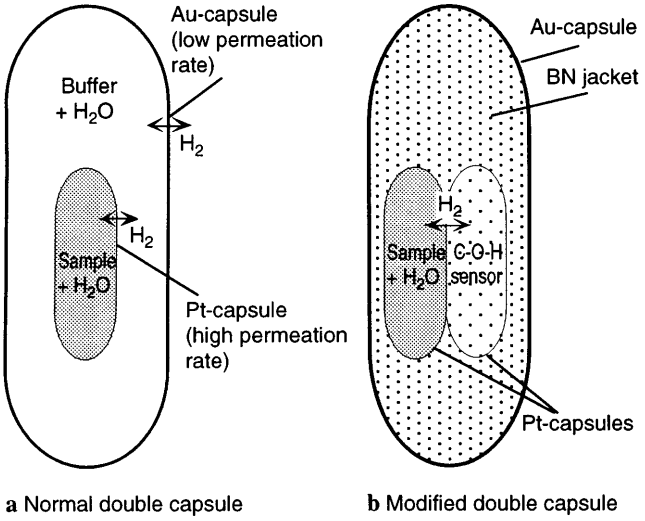

Fig. 1a, b Schematic sketch of normal double-capsule setup and the modified version (outer capsule 8 mm diameter × 50 mm, inner capsule 3 mm diameter × 20 mm, wall thickness 0.2 mm). In the modified setup sensor capsule and sample capsule are in direct contact. Both capsules are enclosed in a BN jacket. Equilibration in f_{H_2} only takes place between the sample and the sensor capsule. The BN prevents rapid loss of hydrogen to the vessel atmosphere

Buffering technique

In high pressure experiments the oxygen fugacity is often controlled using the double-capsule technique described by Eugster and Wones (1962), in which the hydrogen fugacity is set in an outer capsule by the redox equilibrium of a metal and a corresponding metal oxide (e.g. Ni + H_2O = NiO + H_2 for the NNO buffer, Fig. 1). The hydrogen fugacity is buffered by the reaction of metal with water and equilibrates with the atmosphere of the inner sample capsule, setting the oxygen fugacity via the water equilibrium (H_2 + 1/2 O_2 = H_2O). For the inner capsule normally a metal with a high H_2-permeation rate is used and for the outer capsule a metal with a low H_2-permeation rate. At high temperatures, however, the differences in the permeability constants of the metals become smaller (Chou 1986) and only short run durations can be achieved under strongly reducing or oxidising conditions due to rapid hydrogen permeation through the capsule walls.

Using the CSPV at conditions of NNO or CCO the buffer material was enclosed directly into the vessel. The CCO buffer had to be renewed at least every third day due to hydrogen loss from the vessel (Grochau 1996) and the experiments were interrupted once by quenching and reheating. Morphology and major element composition of the plagioclase showed no difference compared to the runs using the NNO buffer which were performed without interruption at the same *P-T* conditions. Thus we infer that the interruption is of minor importance for the resulting partition coefficients.

To quantify f_{O_2} of experiments under intrinsic conditions of the IHPV the redox conditions at 5 MPa and 850 °C were determined using NiPd-solid sensors after Taylor et al. (1992). The obtained value of log f_{O_2} = −10.5 (corresponding to f_{H_2} = 2 bar in the vessel) is in agreement with previous determinations for IHPV (Popp et al. 1984; Linnen et al. 1995).

The conventional double-capsule technique was used at f_{O_2} of NNO and higher. At more reducing conditions hydrogen is rapidly lost from the buffer capsule at the high temperatures used in this study and run durations of several days are not possible. This problem was circumvented by modifying the double-capsule technique. Fig. 1 shows a schematic sketch of the classical double-capsule technique together with the setup used here. Our novel setup is based on the technique used by Truckenbrodt et al. (1997) for piston cylinder apparatus. An oxygen fugacity controlling capsule is placed next to the sample capsule within a boron nitride (BN) jacket which is enclosed in an outer Au capsule. Instead of a buffer assemblage, a C—O—H fluid is used both as hydrogen source and f_{H_2} sensor. During the experiment the assemblage continuously loses hydrogen. However, the use of a BN jacket strongly reduces the loss of hydrogen so that the variation of oxygen fugacity is small during the experiment. As starting material for the sensors organic substances with various H/O ratios are used ($C_9H_{10}O_2$, H/O = 5; $C_{14}H_{22}O$, H/O = 22 or $C_{14}H_{10}$, H/O = ∞). These substances decompose to graphite and a C—O—H fluid (a mixture of CO, CO_2, H_2O, CH_4, C_2H_6), which is analysed by gas chromatography after the run. By summing the amount of H and O in all components of the fluid the total H/O ratio was determined and the hydrogen fugacity calculated using a modified, compensated Redlich Kwong model (Krautheim et al. 1992). The calculation is based on the compensated Redlich Kwong equation of state of Holland and Powell (1991) combined with the mixing rules of De Santis (1974) and the correction of Flowers (1979).

Analytical procedure

Polished sections of the samples were analysed using the Cameca Camebax electron microprobe controlled by the Xmas© software package. The major elements were analysed using standard electron beam conditions, 15 kV, 18 nA. Counting time for each element was 10 s except for Na (5 s). For analyses of the hydrous glass the beam was defocused to 20 μm to avoid Na loss. Elevated exciting conditions (25 kV and 100 nA) were used to obtain accurate analyses of the minor components Eu, Sm and Fe. The concentration of these were determined in separate analyses measuring only these components and using a fixed matrix correction based on the average of the analyses of the major components. Using counting time of 30–60 s the detection limits were in the range of 100 ppm. In both crystals and glasses, the signal intensities for Eu, Sm and Fe show no variation with counting time when monitored for 120 s. Standards were: wollastonite for Si and Ca, albite for Na, corundum for Al, hematite for Fe, europiumphosphate for Eu and samariumphosphate for Sm.

Results and discussion

Improvement of buffering techniques

The stability of the hydrogen fugacity in the modified double-capsule assemblage was investigated by analysing H/O ratios in the sensor capsules and Eu partitioning in the sample capsule as a function of run duration. Figure 2a shows the development of the H/O ratio measured in the sensor capsules. With the exception of two runs, a smooth decrease of the H/O ratio with run duration is observed. In one of the outlying runs the content of organic material in the sensor capsule was only one half of that used in the other runs. In the second outlying run a different temperature path was chosen. The capsule was directly heated to the run temperature whereas the others were held at higher temperature at the beginning of the experiment. This implies that the temperature has large influence on the compaction of the BN and thus on its permeability for hydrogen. Although there is a considerable variation in the H/O ratio and hydrogen fugacity, the resulting oxygen fugacity is quite similar for all run duration. The Eu_2O_3 contents of the coexisting phases and the resulting partition coefficients do not vary significantly with run duration. This indicates that the f_{O_2} was similar for all runs and osmotic equilibrium is reached even for the shortest run duration.

A single run was conducted using anthracene ($C_{14}H_{10}$) as sensor material. As this material is virtually free of oxygen the only oxygen source available is the air enclosed during capsule preparation and water adsorbed on the powder and the capsule wall. In a 48 h experiment at 500 MPa and 850 °C only H_2O was detected as an oxygen bearing fluid species, however, the amount of H_2O was near the detection limit. The H/O-ratio of 798 corresponds to a f_{H_2} of 933 bar for the sensor capsule and log $f_{O_2} = -15.93$ for the sample capsule which is only slightly more reducing than by using $C_{14}H_{22}O$. The lowest hydrogen fugacity which can be achieved theoretically by using organic sensor materials is defined by the graphite-methane buffer.

The mechanism by which the permeability of BN to hydrogen is reduced is not known. In runs using

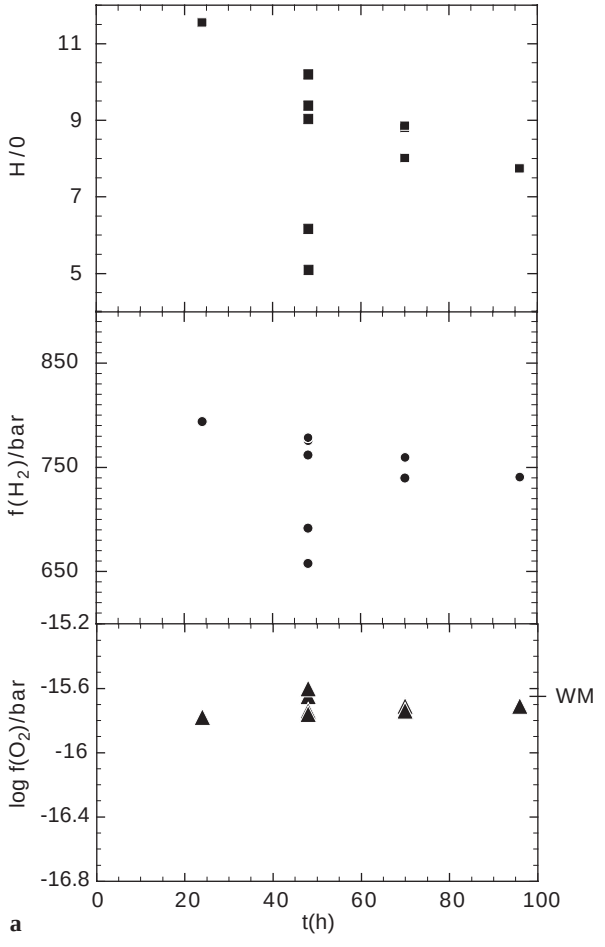

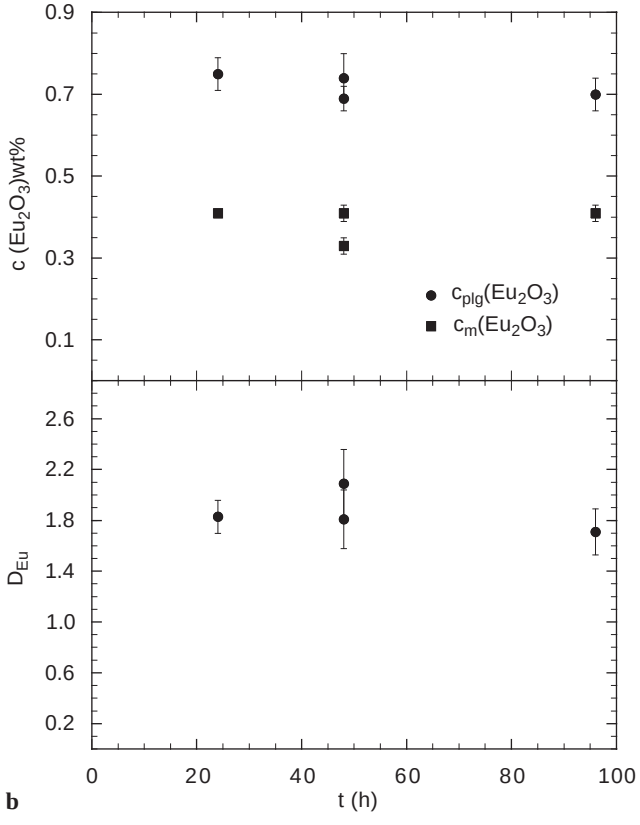

Fig. 2a, b Kinetic experiments at 850 °C and 500 MPa using the BN-jacket technique. **a** Development of H/O ratio, f_{H_2} in the sensor capsule and calculated f_{O_2} in the sample capsule with run duration. The oxygen fugacity in the sample capsule is calculated assuming osmotic equilibrium between sample and sensor capsule and Lewis–Randall mixing of the fluid components in the sample capsule. **b** Eu_2O_3 contents of melt and plagioclase and the resulting partition coefficients versus run duration. Note that both Eu concentrations in the coexisting phases and the partition coefficient show very little variation implying osmotic equilibrium is reached even for the shortest run duration

$C_9H_{10}O_2$ having a low initial H/O we could not detect any hydrogen in the sensor capsule after the run, indicating a high hydrogen permeability of the BN. This implies that the structure of BN is modified by chemical reaction with hydrogen. To investigate the nature of this reaction we used X-ray powder diffraction and Raman spectroscopy. X-ray diffraction analysis on the bulk of the used BN shows no changes compared to the starting material. However, by Raman microspectroscopy the used BN jacket was found to be heterogeneous (Fig. 3). Raman spectra collected by J.M. Beny at the CNRS-CSCM in Orleans (France) using a Dilor XY confocal micro-Raman spectrometer display different features in the centre of the BN jacket, which was light grey, and on the outer rim, which was black. The peak at 1365 cm^{-1} of crystalline BN is still visible for the inner part of the BN but is absent for the outer part. In both parts new bands appear at ≈1600 cm^{-1} and ≈2800 cm^{-1}. Additional bands at ≈830 cm^{-1} and ≈1800 cm^{-1} are visible in the spectrum of the inner part. Despite the origin of the new bands is not well known, the spectra clearly demonstrate alteration of the BN during the experiments. We suggest that the formation of new phases by reaction with hydrogen favours the compaction of BN resulting in a low hydrogen permeability.

It might be expected that the compaction of the BN results in pressure shielding of the sample capsule. Thus the effective pressure on the sample might be lower than the external pressure. However, water contents of glasses, estimated by the totals of microprobe analyses, are in good agreement for experiments using BN jackets and other experiments (mean totals: 89.11 ± 1.31 for BN runs compared to 88.12 ± 0.74 for the other runs). The estimated water contents are close to water solubilities determined at 1200 °C and 500 MPa for tonalitic melts by Grams and Behrens (1996). Therefore we infer that the differences in pressure of the experiments are below 50 MPa.

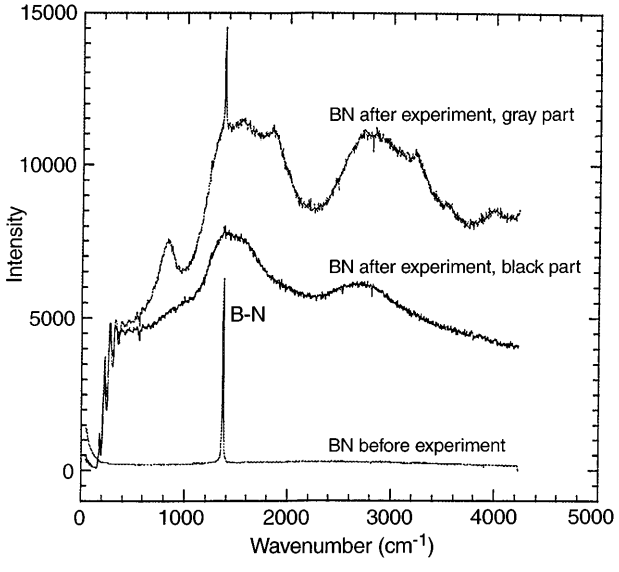

Fig. 3 Raman Spectra recorded on the central, grey part and the outer, black part of an used BN jacket. A spectrum of the original BN is shown for comparison. The sharp peak at 1365 cm^{-1} of crystalline BN vanishes and several broad bands appear. For details see text

Reaction kinetics and achievement of chemical equilibrium

Figure 4a shows a BSE image of a charge run at 850 °C/ 500 MPa using a rate of 1°/min for cooling from liquidus to crystallisation temperature (900° ↔ 850 °C). The crystals contain some melt inclusions and have skeletal shapes, indicating rapid, disequilibrium growth. Formation of melt inclusions in the plagioclase and skeletal crystal growth are negligible with a cooling rate of 0.5°/min (Fig. 4b), so this cooling rate was used in the subsequent runs. The phases show no systematic variations in either major or minor components, neither the crystals (rim and core) nor the glass (Table 2). From the euhedral crystal shape and the absence of zoning in the crystals we conclude that the plagioclase was formed by near equilibrium growth.

Kinetic parameters which might influence the partitioning of the heterovalent cations are (i) redox equilibration of the sample with the buffer, (ii) nucleation and growth of crystals and (iii) diffusion of components in the melt.

Permeation of hydrogen through the capsule wall is fast even at 750 °C. The times to transport the amount of hydrogen necessary to set up the redox conditions in the sample capsule calculated after Chou (1986) are in the range of 30–70 s for Pt capsules and NNO buffer. Even for Au the times are in the range of only 300–700 s. Transport rates are not well known for hydrogen and oxygen in hydrous silicate melts. Experimental observations on H_2 and H_2O bearing glasses indicate that the diffusivity of hydrogen is orders of magnitude higher than the diffusivity of water (Schmidt 1996; Gaillard et al. 1998). This suggests that the redox conditions are established throughout the sample within a few minutes.

Time dependent experiments have shown continuous growth of plagioclase over several days at 750 °C and 850 °C. At 850 °C using the retrograde temperature path with a slower cooling rate (0.5 °C/min) plagioclase crystals with a size of 10 μm are found even in runs quenched directly after cooling to the crystallisation temperature. These crystals have nucleated and grown during the cooling period (100 min) preferentially close to the surface of the melt body. The An content is similar to those of the 48 h runs (An_{73}). However, the partition coefficient for Eu is significantly lower in short term experiments and increases with run duration (for intrinsic conditions: D_{Eu} = 0.38 directly after reaching run temperature, D_{Eu} = 0.50 after 4 h, D_{Eu} = 0.77 after 48 h). The partition coefficients at the beginning are too small to be explained by initially higher temperature during crystallisation. We suggest that the low partition coeffi-

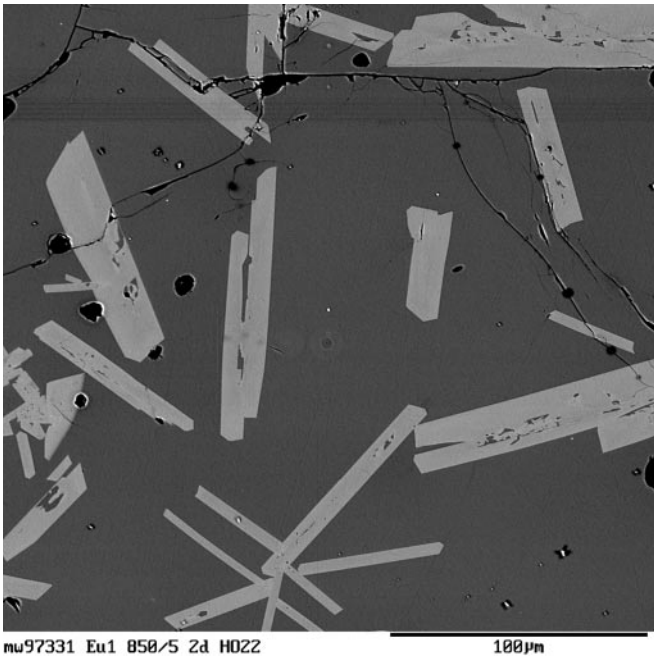

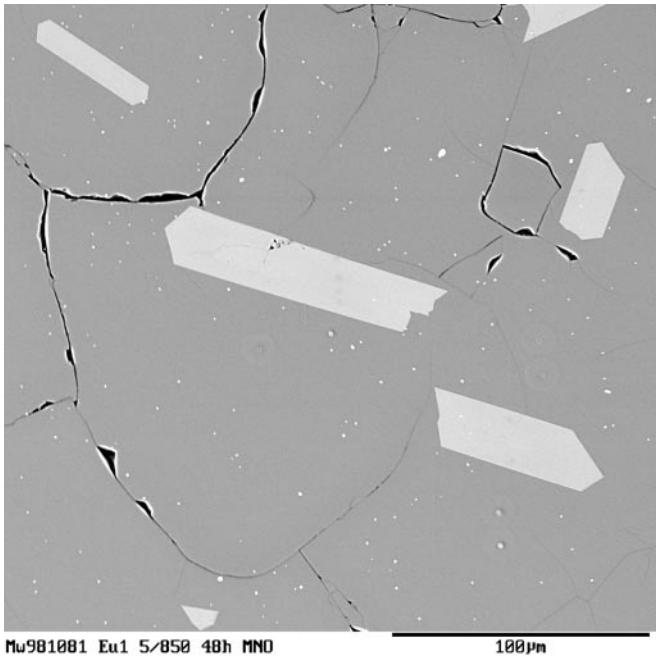

Fig. 4a, b Back scattered electron images of run products at 850 °C and 500 MPa. *Dark areas* melt, *bright areas* plagioclase. **a** (left) Temperature path: 30 °C/min to 900 °C – 30 min at 900 °C – 1 °C/min to 850 °C – 48 h at 850 °C. **b** (right) 30 °C/min to 900 °C – 30 min at 900 °C – 0.5 °C/min to 850 °C – 48 h at 850 °C

cients result from more oxidising conditions prevailing in the melt at the beginning of the experiment. This is in accordance with observations made by Gaillard et al. (1998), who found that the change in the redox state is not as fast as expected from the rapid hydrogen diffusion in the melt. A possible explanation is that the solubility of hydrogen in the melt is small and thus the transport rate of hydrogen (which is controlling the redox reaction) is small. The time dependent experiments at the most reducing conditions demonstrate that equilibrium partitioning is achieved for run durations ≥24 h. No relicts of the initially formed plagioclase with low Eu contents could be found in the long duration runs.

At 750 °C plagioclase is firstly observed after 60 min using a retrograde temperature path (30 min at 830 °C–3 °C/min to 750 °C). Even after 4 h the crystals were too small (< 2 µm) for microprobe analysis. The maximum size after 4 days was about 80 × 30 µm. No systematic investigations were performed to prove equilibrium partitioning for this temperature because of the slow crystallisation kinetics. We assume that a run duration of 4 days is sufficient to achieve near equilibrium conditions.

Partitioning of Eu and Sm

Compositions of plagioclase and melt and the calculated partition coefficients and major component compositions are shown in Table 2 and 3. At 850 °C the D value for Eu (Fig. 5a) varies in the investigated f_{O_2} range from 0.095 for oxidising conditions (Cu—Cu_2O buffer) to 1.81 for the most reducing conditions (C—O—H sensor). The D_{Sm} does not vary with oxygen fugacity and has an average value of 0.07. Using the Cu—Cu_2O buffer Eu and Sm have similar partition coefficients. It can be expected that more oxidising conditions give no significant changes for the Eu partitioning. Decreasing the temperature to 750 °C for a given f_{O_2} the partition coefficient of Eu is strongly decreased at intermediate oxygen fugacities (Fig. 5a), e.g. by a factor of 2.0 for log $f_{O_2} = -11$. It is emphasised that for a given buffer condition the effect of temperature is small as the equilibrium f_{O_2} of the buffer also changes with temperature. At MnO—Mn_3O_4 the partition coefficient is even independent on temperature. This insensitivity of D_{Eu} to temperature on a relative f_{O_2} scale (e.g. ΔNNO = $\log(f_{O_2}/f_{O_2 NHO})$) is important for the geological application of the experimental data since the temperature of formation of natural rocks is often not known very precisely.

D_{Eu} and D_{Sm} determined by Weill and McKay (1975) in 1 atm experiments at 1200 °C in lunar basaltic rocks are similar to our data for a given f_{O_2} (Fig. 5a). For terrestrial basaltic and andesitic compositions Drake and Weill (1975) found higher partition coefficients for REE than for lunar basalts (e.g. for Sm by a factor 2.5 at 1200 °C). The differences are attributed by Weill and McKay (1975) to the composition of the melt. Partitioning of Eu in terrestrial basalts and andesites at 1200 °C and 1 atm (Drake and Weill 1975) is for a given f_{O_2} higher than for hydrous tonalitic melts at 850 °C and 500 MPa. Using the Arrhenius equations determined by Drake and Weill (1975) for the T range 1150–1400 °C to calculate the partition coefficients of Sm and Eu at 850 °C gives $D_{Sm} = 0.13$ and $D_{Eu} = 0.10$ (in air). The extrapolated value for Sm is higher by approximately a

Table 2 Compositions of run products from representative experiments. In parentheses 1s standard deviation is given. Equilibrium-oxygen fugacities of buffer are calculated using data of Robie and Hemingway (1995). Low sums of glass analyzes are due to approx. 11 wt% water dissolved

To1 (Eu) 500 MPa, 850 °C

Sample	68		136		108		13		86		57	
Buffer	Cu—Cu_2O		Fe_2O_3—Fe_3O_4		MnO—Mn_3O_4		Intrinsic		Ni—NiO		C—O—H Sensor	
$\log(f_{O_2}/\text{bar})$	−7.27		−8.54		−9.00		−10.5		−12.74		−15.72	
Phase	Plg	Gls	Plg	Gls	Plg	Gls	Plg	Gls	Plg	Gls	Plg	Gls
SiO_2	49.40 (0.35)	65.90 (0.56)	50.40 (0.50)	65.21 (0.29)	50.64 (0.47)	64.49 (0.14)	50.84 (0.53)	65.15 (0.27)	49.20 (0.71)	64.61 (0.34)	50.77 (0.64)	68.06 (0.47)
Al_2O_3	32.36 (0.25)	14.40 (0.16)	31.43 (0.32)	14.45 (0.13)	31.27 (0.24)	14.86 (0.19)	31.88 (0.44)	14.59 (0.20)	31.95 (0.51)	14.32 (0.11)	31.67 (0.44)	14.22 (0.16)
CaO	15.52 (0.27)	5.11 (0.10)	14.99 (0.43)	5.15 (0.07)	14.45 (0.32)	5.66 (0.04)	15.08 (0.32)	5.41 (0.07)	15.07 (0.59)	5.04 (0.06)	14.55 (0.46)	4.92 (0.08)
Na_2O	2.91 (0.23)	2.88 (0.06)	3.12 (0.24)	2.90 (0.15)	3.34 (0.21)	2.88 (0.02)	3.15 (0.21)	2.60 (0.14)	2.76 (0.22)	2.83 (0.14)	3.23 (0.18)	2.74 (0.11)
Eu_2O_3	0.05 (0.01)	0.36 (0.04)	0.079 (0.007)	0.35 (0.01)	0.11 (0.01)	0.37 (0.01)	0.37 (0.02)	0.48 (0.01)	0.36 (0.02)	0.39 (0.01)	0.70 (0.04)	0.41 (0.02)
Sm_2O_3	0.04 (0.01)	0.36 (0.07)	0.020 (0.005)	0.33 (0.01)	0.02 (0.01)	0.35 (0.02)	0.03 (0.01)	0.53 (0.03)	0.03 (0.01)	0.36 (0.01)	0.04 (0.01)	0.48 (0.02)
Total	100.28	89.01	100.04	88.39	99.83	88.61	101.35	88.76	99.37	87.55	100.96	90.83
Qz		43		43		40		44		43		46
Ab[a]	25	28	27	28	29	28	27	25	25	28	29	26
An[a]	75	29	73	29	71	32	73	31	75	29	71	27
C												1
D_{Eu}	0.116 ± 0.028		0.226 ± 0.026		0.297 ± 0.035		0.771 ± 0.058		0.92 ± 0.075		1.71 ± 0.18	
D_{Sm}	0.098 ± 0.017		0.061 ± 0.017		0.057 ± 0.032		0.057 ± 0.022		0.08 ± 0.030		0.083 ± 0.024	

Tol (Fe) 500 MPa, 850 °C

Sample	77		92		109		98		107		66	
Buffer	Cu—Cu_2O		Fe_2O_3—Fe_3O_4		MnO—Mn_3O_4		Intrinsic		Ni—NiO		C—O—H Sensor	
$\log(f_{O_2}/\text{bar})$	−7.27		−8.54		−9.00		−10.5		−12.74		−15.88	
Phase	Plg	Gls	Plg	Gls	Plg	Gls	Plg	Gls	Plg	Gls	Plg	Gls
SiO_2	51.02 (1.21)	66.77 (0.64)	50.50 (0.24)	65.04 (0.15)	50.73 (0.37)	62.45 (0.43)	49.98 (0.41)	64.32 (0.17)	50.35 (0.20)	65.35 (0.30)	49.53 (0.48)	66.40 (0.36)
Al_2O_3	31.05 (0.69)	13.92 (0.12)	31.47 (0.19)	14.74 (0.24)	30.90 (0.27)	15.06 (0.05)	31.72 (0.43)	14.30 (0.14)	31.36 (0.15)	15.11 (0.08)	32.25 (0.28)	14.12 (0.18)
CaO	14.40 (0.69)	4.96 (0.05)	14.83 (0.16)	5.39 (0.08)	14.53 (0.20)	6.59 (0.04)	15.32 (0.43)	5.44 (0.12)	14.64 (0.17)	5.60 (0.11)	15.11 (0.37)	5.16 (0.17)
Na_2O	3.42 (0.45)	2.39 (0.23)	2.95 (0.08)	2.43 (0.10)	3.32 (0.05)	2.51 (0.17)	3.38 (0.29)	2.63 (0.08)	3.31 (0.06)	2.32 (0.10)	2.86 (0.19)	2.22 (0.19)
$Fe_2O_{3,tot}$	0.41 (0.08)	1.00 (0.10)	0.39 (0.05)	0.84 (0.04)	0.32 (0.05)	0.92 (0.04)	0.17 (0.01)	0.94 (0.06)	0.10 (0.01)	0.87 (0.04)	0.08 (0.01)	0.94 (0.05)
Total	100.31	89.04	100.14	88.44	99.80	87.53	100.57	87.63	99.76	89.25	99.83	88.84
Qz		48		45		39		43		45		48
Ab[a]	30	23	27	23	29	24	29	26	29	22	26	21
An[a]	70	28	73	31	71	37	71	31	71	31	74	29
C		1		1						1		1
D_{Fe}	0.600 ± 0.138		0.46 ± 0.08		0.380 ± 0.027		0.181 ± 0.022		0.118 ± 0.015		0.085 ± 0.013	

To2 (Eu) 500 MPa, 750 °C

Sample	156		120		111		151		85	
Buffer	Cu—Cu_2O		Fe_2O_3—Fe_3O_4		MnO—Mn_3O_5		Ni—NiO		Co—CoO	
$\log(f_{O_2}/\text{bar})$	−8.74		−10.90		−10.96		−14.84		−16.15	
Phase	Plg	Gls	Plg	Gls	Plg	Gls	Plg	Gls	Plg	Gls
SiO_2	51.20 (0.49)	67.33 (0.72)	51.03 (0.23)	67.13 (0.20)	50.75 (0.26)	66.44 (0.22)	52.36 (0.48)	67.80 (0.21)	52.64 (0.64)	68.40 (0.35)
Al_2O_3	31.08 (0.09)	12.97 (0.18)	31.43 (0.28)	13.08 (0.11)	30.84 (0.26)	12.56 (0.13)	30.29 (0.32)	12.43 (0.05)	29.60 (0.47)	12.38 (0.14)
CaO	14.31 (0.08)	4.89 (0.07)	14.55 (0.19)	5.41 (0.04)	14.48 (0.15)	5.37 (0.05)	13.31 (0.35)	4.56 (0.06)	12.47 (0.44)	4.96 (0.05)
Na_2O	3.44 (0.10)	1.96 (0.08)	3.43 (0.13)	1.91 (0.09)	3.22 (0.10)	1.54 (0.16)	3.80 (0.17)	2.34 (0.09)	4.01 (0.28)	1.87 (0.12)
Eu_2O_3	0.09 (0.02)	0.57 (0.01)	0.09 (0.01)	0.30 (0.01)	0.13 (0.01)	0.45 (0.02)	0.73 (0.03)	0.64 (0.02)	0.85 (0.08)	0.64 (0.01)
Total	100.12	87.73	100.44	87.83	99.78	86.36	100.49	87.77	99.57	88.25
Qz		52		51		54		51		54
Ab[a]	30	19	30	18	29	15	34	23	37	18
An[a]	70	28	70	31	71	31	66	26	63	28
C		1								
D_{Eu}	0.158 ± 0.038		0.300 ± 0.043		0.289 ± 0.035		1.18 ± 0.09		1.44 ± 0.16	

To2 (Fe) 500 MPa, 750 °C

Sample	157		137		114		150		83		148	
Buffer	Cu—Cu_2O		Fe_2O_3—Fe_3O_4		MnO—Mn_3O_5		Ni—NiO		Co—CoO		C—O—H Sensor	
$\log(f_{O_2}/\text{bar})$	−8.74		−10.90		−10.96		−14.84		−16.15		−17.62	
Phase	Plg	Gls	Plg	Gls	Plg	Gls	Plg	Gls	Plg	Gls	Plg	Gls
SiO_2	52.33 (0.51)	67.83 (0.38)	51.75 (0.60)	67.45 (0.11)	53.58 (0.20)	66.84 (0.31)	51.45 (0.30)	67.94 (0.20)	52.56 (0.28)	67.18 (0.17)	51.83 (0.60)	66.48 (0.26)
Al_2O_3	30.38 (0.23)	12.72 (0.18)	30.09 (0.19)	12.54 (0.15)	28.96 (0.13)	12.68 (0.11)	31.05 (0.32)	12.73 (0.07)	30.17 (0.18)	12.88 (0.08)	30.22 (0.41)	12.87 (0.12)
CaO	14.05 (0.23)	5.25 (0.09)	13.68 (0.25)	4.88 (0.05)	12.51 (0.18)	4.93 (0.04)	14.32 (0.23)	4.91 (0.08)	13.15 (0.15)	4.89 (0.07)	13.18 (0.29)	5.12 (0.09)
Na_2O	3.75 (0.12)	1.89 (0.21)	3.74 (0.20)	1.85 (0.17)	4.31 (0.04)	1.34 (0.29)	3.53 (0.16)	1.57 (0.29)	4.09 (0.10)	1.98 (0.16)	3.83 (0.19)	1.79 (0.15)
$Fe_2O_{3,tot}$	0.53 (0.03)	0.67 (0.08)	0.46 (0.04)	0.88 (0.03)	0.42 (0.04)	1.00 (0.07)	0.23 (0.04)	1.61 (0.06)	0.14 (0.01)	1.41 (0.07)	0.14 (0.02)	1.40 (0.05)
Total	101.04	88.37	99.72	87.60	99.78	86.79	100.58	88.76	100.11	88.34	99.21	87.66
Qz		52		53		56		56		52		52
Ab[a]	33	18	33	18	38	13	31	15	36	19	34	18
An[a]	67	30	67	28	62	29	69	28	64	28	66	29
C				1		2		1		1		1
D_{Fe}	0.791 ± 0.139		0.523 ± 0.063		0.420 ± 0.069		0.143 ± 0.030		0.099 ± 0.012		0.100 ± 0.018	

[a] Feldspar components are in mol% for crystals and in wt% for glass.

factor of 2 than our experimental value. For Eu, however, the predicted value is quite similar to our data measured at most oxidising conditions.

Partitioning of Fe

In the investigated f_{O_2} range the variation of element partitioning with f_{O_2} is significantly smaller for Fe than for Eu (Fig. 5b). At 850 °C and 500 MPa D_{Fe} for partitioning between plagioclase and hydrous tonalitic melt varies from 0.08 at C—O—H sensor to 0.55 at Cu—Cu_2O buffer. In contrast to the case for Eu, lowering the temperature to 750 °C increases the partition coefficient of Fe for a given oxygen fugacity, e.g. by a factor of 2.2 for log f_{O_2} = −11. As observed for Eu, in the experimental range the effect of temperature is more pronounced at intermediate oxygen fugacities. Furthermore for a given buffer the effect of temperature is relatively small also for D_{Fe}.

Compared to high temperature experiments in basaltic systems of Sato (1989) and Phinney (1992) our data are shifted to higher D values for a given f_{O_2} (Fig. 5b). From the experimental data available so far we cannot clarify whether these differences are due to temperature or melt composition.

Modelling the partitioning data

The partitioning data can be modelled using the redox equilibrium of the heterovalent cations in the melt and assuming independent partitioning for divalent and trivalent cations. The redox reaction between divalent and trivalent cations in the melt can be written as:

$$MO + \frac{1}{4}O_2 = MO_{1.5} \quad M = Fe, Eu \tag{1}$$

The equilibrium constant K_m for this reaction is,

$$K_m = \frac{a_{MO_{1.5},m}}{a_{MO,m} \cdot f_{O_2}^{1/4}} \tag{2}$$

where a denotes the activity of the respective components in the melt. Using $a_i = \gamma_i x_i$ (γ_i = activity coefficient; x_i = mole fraction of component i) and assuming $\gamma_{MO} = \gamma_{MO_{1.5}}$ we can rewrite the equilibrium reaction on the basis of mole fractions:

$$K_m = \frac{(x_{MO_{1.5}}/x_{MO})_m}{f_{O_2}^{1/4}} \quad . \tag{3}$$

Partition coefficients usually are given on the basis of weight percent. Rewriting Eq. 3 in terms of mass fractions of the heterovalent cations (given in brackets) results in:

$$K_m = \frac{[M^{3+}]_m/[M^{2+}]_m}{f_{O_2}^{1/4}} \tag{4}$$

The partition coefficient can be written as follows:

$$D_M = \frac{[M^{2+}]_{plg} + [M^{3+}]_{plg}}{[M^{2+}]_m + [M^{3+}]_m} = \frac{\frac{[M^{2+}]_{plg}}{[M^{2+}]_m} + \frac{[M^{3+}]_{plg}}{[M^{2+}]_m}}{1 + \frac{[M^{3+}]_m}{[M^{2+}]_m}} \quad . \tag{5}$$

Combining Eqs. 5 and 4 gives

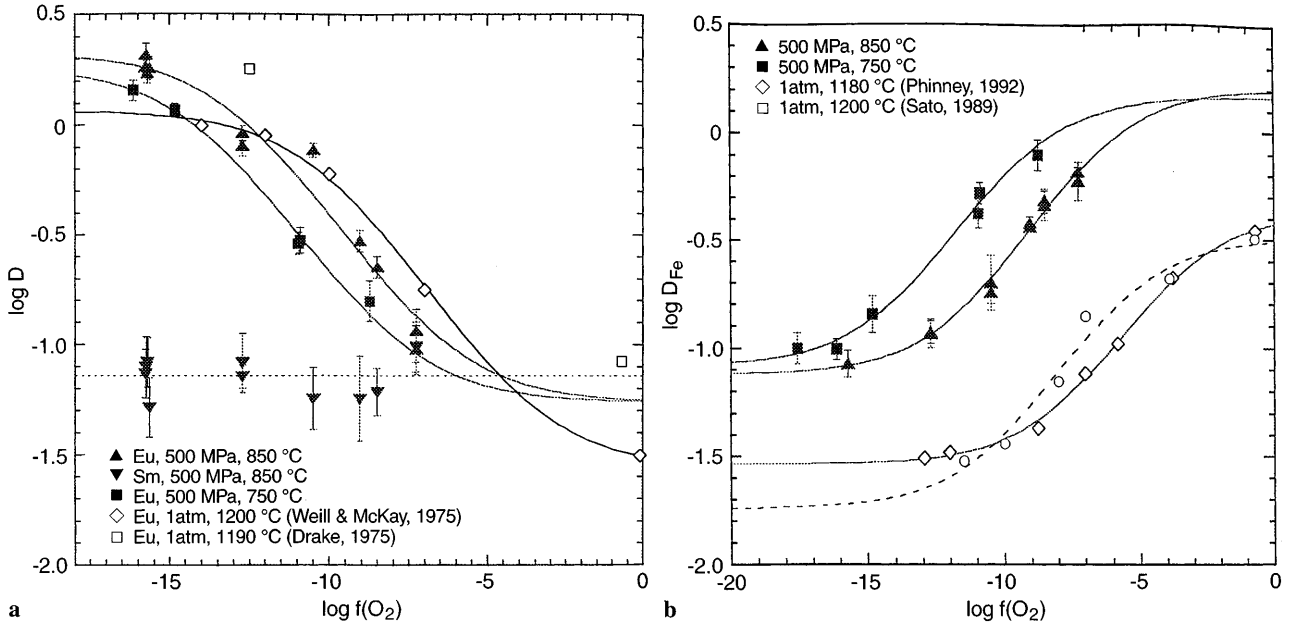

Fig. 5a, b Variation of the partition coefficients of Eu and Sm (**a**, left) and Fe (**b**, right) with log f_{O_2}. For comparison data on Eu partitioning (Weill and McKay 1975; Drake 1975) and Fe partitioning (Sato 1989; Phinney 1992) for basaltic compositions at 1180–1200 °C and 1 atm are shown. Curves were calculated using Eq. 7 and the fit parameters in Table 4 (for details see text)

Table 3 Average concentrations of Eu, Sm and Fe for plagioclase and glass and the derived partition coefficients of all experiments shown in the figures

Exp. No.	T (°C)	log f_{O_2}	Eu_2O_3 Plg	Eu_2O_3 Gls	Sm_2O_3 Plg	Sm_2O_3 Gls	D_{Eu}	D_{Sm}
68	850	−7.27	0.05 (0.01)	0.36 (0.04)	0.04 (0.01)	0.36 (0.07)	0.116 ± 0.028	0.098 ± 0.029
59	850	−7.27	0.04 (0.01)	0.42 (0.02)	0.040 (0.005)	0.41 (0.01)	0.095 ± 0.028	0.098 ± 0.017
136	850	−8.54	0.079 (0.007)	0.35 (0.01)	0.020 (0.005)	0.33 (0.01)	0.226 ± 0.026	0.061 ± 0.017
108	850	−9.00	0.11 (0.01)	0.37 (0.01)	0.02 (0.01)	0.35 (0.02)	0.297 ± 0.035	0.057 ± 0.032
13	850	−10.50	0.37 (0.02)	0.48 (0.01)	0.03 (0.01)	0.53 (0.03)	0.771 ± 0.058	0.057 ± 0.022
86	850	−12.74	0.36 (0.02)	0.39 (0.01)	0.03 (0.01)	0.36 (0.01)	0.920 ± 0.075	0.083 ± 0.030
87	850	−12.74	0.36 (0.02)	0.45 (0.02)	0.036 (0.003)	0.50 (0.02)	0.810 ± 0.089	0.072 ± 0.009
57	850	−15.71	0.70 (0.04)	0.41 (0.02)	0.04 (0.01)	0.48 (0.02)	1.71 ± 0.18	0.083 ± 0.024
33	850	−15.65	0.74 (0.06)	0.41 (0.02)	0.03 (0.01)	0.58 (0.02)	1.81 ± 0.23	0.052 ± 0.019
48	850	−15.75	0.69 (0.03)	0.33 (0.02)	0.03 (0.01)	0.38 (0.02)	2.09 ± 0.27	0.079 ± 0.030
58	850	−15.78	0.75 (0.04)	0.41 (0.01)	0.04 (0.01)	0.54 (0.02)	1.83 ± 0.13	0.074 ± 0.021
156	750	−8.74	0.09 (0.02)	0.57 (0.01)			0.158 ± 0.038	
120	750	−10.90	0.09 (0.01)	0.30 (0.01)			0.300 ± 0.043	
111	750	−10.96	0.13 (0.01)	0.45 (0.02)			0.289 ± 0.035	
151	750	−14.84	0.73 (0.03)	0.64 (0.02)			1.18 ± 0.09	
85	750	−16.15	0.64 (0.01)	0.85 (0.08)			1.44 ± 0.16	

Exp. No.	T (°C)	log f_{O_2}	$Fe_2O_{3,tot}$ Plg	$Fe_2O_{3,tot}$ Gls	D_{Fe}
60	850	−7.27	0.46 (0.02)	0.70 (0.01)	0.660 ± 0.038
77	850	−7.27	0.41 (0.08)	1.00 (0.10)	0.600 ± 0.138
92	850	−8.54	0.39 (0.05)	0.84 (0.04)	0.460 ± 0.080
110	850	−8.54	0.82 (0.07)	1.69 (0.09)	0.485 ± 0.067
123	850	−9.00	0.62 (0.02)	1.78 (0.05)	0.365 ± 0.018
109	850	−9.00	0.32 (0.05)	0.92 (0.04)	0.380 ± 0.027
90	850	−10.50	0.18 (0.04)	0.88 (0.11)	0.200 ± 0.068
98	850	−10.50	0.17 (0.01)	0.94 (0.06)	0.181 ± 0.022
107	850	−12.74	0.10 (0.01)	0.87 (0.04)	0.118 ± 0.015
99	850	−12.74	0.11 (0.01)	0.94 (0.07)	0.117 ± 0.019
66	850	−15.74	0.08 (0.01)	0.94 (0.05)	0.085 ± 0.013
157	750	−8.74	0.53 (0.03)	0.67 (0.08)	0.791 ± 0.139
137	750	−10.90	0.46 (0.04)	0.88 (0.03)	0.523 ± 0.063
114	750	−10.96	0.42 (0.04)	1.00 (0.07)	0.420 ± 0.069
150	750	−14.84	0.23 (0.04)	1.61 (0.06)	0.143 ± 0.030
83	750	−16.15	0.14 (0.01)	1.41 (0.07)	0.099 ± 0.012
148	750	−17.61	0.14 (0.02)	1.40 (0.05)	0.100 ± 0.018

$$D_M = \frac{D_{M^{2+}} + D_{M^{3+}} \cdot K_m \cdot f_{O_2}^{1/4}}{1 + K_m \cdot f_{O_2}^{1/4}} \quad (6)$$

where $D_{M^{3+}}$, and $D_{M^{2+}}$ denote the partition coefficients of the two cations.

Equation 6 describes the dependence of the partition coefficient on oxygen fugacity. The three parameters $D_{M^{2+}}$ $D_{M^{3+}}$ and K_m were determined by fitting the partitioning data using a plot of log D versus log f_{O_2}.

$$\log D_M = \log \frac{D_{M^{2+}} + D_{M^{3+}} \cdot K_m \cdot 10^{1/4 \log f_{O_2}}}{1 + K_m \cdot 10^{1/4 \log f_{O_2}}} \quad (7)$$

It is emphasised that Eqs. 5 and 6 only are valid if the activity coefficients of the two melt components MO and $MO_{1.5}$ are identical but does not necessarily require ideal mixing of components in the melt. As the composition of coexisting melt and plagioclase does not change in the investigated f_{O_2}-range the activities of the components in melt and crystals are constant, and therefore $D_{M^{2+}}$ and $D_{M^{3+}}$ do not vary with f_{O_2}. Thus, the f_{O_2}-dependance of Eu and Fe partition coefficients are expected to be controlled by the redox ratio of the elements in the melt, only.

In Figs. 5a and 5b the experimentally derived data are shown together with the fitted functions for Eu and Fe at 850 °C, respectively. For both elements the fit is poorly constrained for very oxidising conditions. Without extra constrains the fit of the Eu data extends to negative values for $D_{Eu^{3+}}$, a nonsensical result. Unfortunatety, all attempts to perform experiments at very oxidising conditions (Mn_3O_4—Mn_2O_3) failed due to rapid consumption of the buffer material. Therefore the $D_{Eu^{3+}}$ value was estimated using the measured D for the Sm partitioning. The ratio of the partition coefficients for Sm and Eu was derived by extrapolating the data given by Drake and Weill (1975) (D_{Sm}/D_{Eu} = 1.3 at 850 °C). Thus for the fit of the Eu data $D_{Eu^{3+}}$ was set to 0.055. At 750 °C the partition coefficient for Sm was not determined experimentally. But as the partition coefficient of Sm at 950 °C does not differ from the one at 850 °C within the error of the analyses (Wilke 1999) the data were fitted assuming a T independent D value for

Eu^{3+}. With these constrains the experimental data of Eu are well reproduced except for one outlying value at 850 °C and log $f_{O_2} = -10.5$, probably because f_{O_2} was not well defined in this unbuffered experiment. The results of modelling the partitioning data imply that $D_{Eu^{2+}}$ increases whereas $K_{m,Eu}$ decreases with increasing temperature (Table 4).

Experimental Fe partitioning data are well fitted without any constrain on $D_{Fe^{3+}}$ and $D_{Fe^{2+}}$. The values for $D_{Fe^{3+}}$ and $D_{Fe^{2+}}$ derived from the Fe partitioning data at 750 °C agree, within experimental error, with the values obtained at 850 °C indicating that the observed change in Fe partitioning with temperature results mainly from the decreasing $K_{m,Fe}$ with increasing temperature. The observed T dependence of M^{3+}/M^{2+} is in accordance with results of previous studies on silicate melts in that the divalent cation is favoured at high temperature (e.g. Fudali 1965; Morris et al. 1974; Sack et al. 1980).

The same model was applied to the data for Fe partitioning (Sato 1989; Phinney 1992) and Eu partitioning (Weill and Mckay 1975) between plagioclase and basaltic melts. Slightly different parameters are obtained for Fe partitioning in basaltic melts using the data of Sato (1989) and Phinney (1992), which might be attributed to different bulk compositions used in both studies. The starting glass used by Phinney has higher FeO but lower MgO and CaO contents. For both, Fe and Eu partitioning the resulting values for $D_{M^{3+}}$ and $D_{M^{2+}}$ as well as K_m are lower for basaltic melts at ≈1200 °C and 1 atm than for the tonalitic melts at 850 °C/500 MPa data. With the available data it is not possible to decide whether the differences of the parameters are due to melt composition, temperature, pressure or combinations of these.

Redox state of the melt

M^{3+}/M^{2+} ratios calculated from the partitioning data for the tonalitic melts at 750 and 850 °C and at 500 MPa are plotted in Fig. 6a. Due to larger scattering of the experimental data and to the constrains made for fitting, the redox ratios for Eu are less reliable than those for Fe. Nevertheless, it is evident that for a given f_{O_2} and temperature Eu^{3+}/Eu^{2+} is more than one order of magnitude larger than Fe^{3+}/Fe^{2+}.

When we compare the ferric-ferrous ratios determined from the partitioning data with those predicted by the empirical calculation model of Kress and Carmichael (1991), the absolute values are different (up to an order of magnitude at reducing conditions) as well as the f_{O_2} dependence (Fig. 6a). The ferric-ferrous ratios in the melts calculated from Fe partitioning are supported by preliminary results of ^{57}Fe-Moessbauer spectroscopy on tonalitic glasses equilibrated at the same experimental conditions (Wilke and Behrens 1998). This implies that the calculation model of Kress and Carmichael (1991) must be revised for application to low temperature magmatic systems. On the other hand, a much better agreement of ferric-ferrous ratios extracted from partitioning data with those calculated from the Kress and Carmichael model is obtained using the high temperature data of Phinney (1992) and Sato (1989) (Fig. 6b). This suggests that the Kress and Carmichael model is more suitable for estimating ferric-ferrous ratios of magmatic melts at high temperature, however, our results imply that the f_{O_2} dependence might be larger than predicted by the empirical model.

Application: an oxygen barometer for magmatic systems?

A strong dependence of Fe and Eu partitioning between plagioclase and hydrous tonalitic melts on f_{O_2} is observed between NNO and NNO + 4. In this f_{O_2} range D_{Fe} increases by around 0.10 log units and D_{Eu} decreases by ~0.13 log units per log unit of f_{O_2} at 850 °C and 500 MPa. This implies that Fe and Eu partitioning may be used as an sensitive oxygen barometer for magmatic processes. Preeruptive redox conditions in magma chambers have been estimated from Fe-Ti oxides and phase relationships between NNO + 0.4 and NNO + 0.8 for Mt. Pelee (Martel et al. 1998) and close to NNO + 1.7 for Pinatubo (Evans and Scaillet 1997), i.e. in the range where the partitioning of Eu and Fe is very sensitive to f_{O_2}. Thus measurements on plagioclase and on glass inclusions in the plagioclase might further constrain the oxygen fugacity during the differentiation in the magma chamber.

Oxygen fugacities can be calculated from partition coefficients of Fe and Eu after rearrangement of Eq. 7:

Table 4 Fit parameter and standard error (given in brackets) obtained for Eq. 7 using the datasets shown

	Eu this study 500 MPa/750 °C Tonalite	Eu this study 500 MPa/850 °C Tonalite	Eu Weill and Mckay (1975) 1 atm, 1200 °C Basalt	Fe this study 500 MPa/750 °C Tonalite	Fe this study 500 MPa/850 °C Tonalite	Fe Phinney (1992) 1 atm, 1180 °C Basalt	Fe Sato (1989) 1 atm, 1200 °C Basalt
$D_{M^{2+}}$	1.85 (0.17)	2.14 (0.31)	1.16 (0.07)	0.083 (0.009)	0.078 (0.006)	0.029 (0.001)	0.0018 (0.006)
$D_{M^{3+}}$	0.055[a]	0.055[a]	0.028 (0.002)	1.47 (0.41)	1.7 (0.5)	0.42 (0.03)	0.32 (0.06)
K_m	3198 (489)	1650 (420)	349 (44)	207 (99)	37 (16)	7.20 (0.95)	25.0 (9.9)
R^2	0.993	0.961	0.999	0.992	0.991	0.998	0.978

[a] Fixed value.

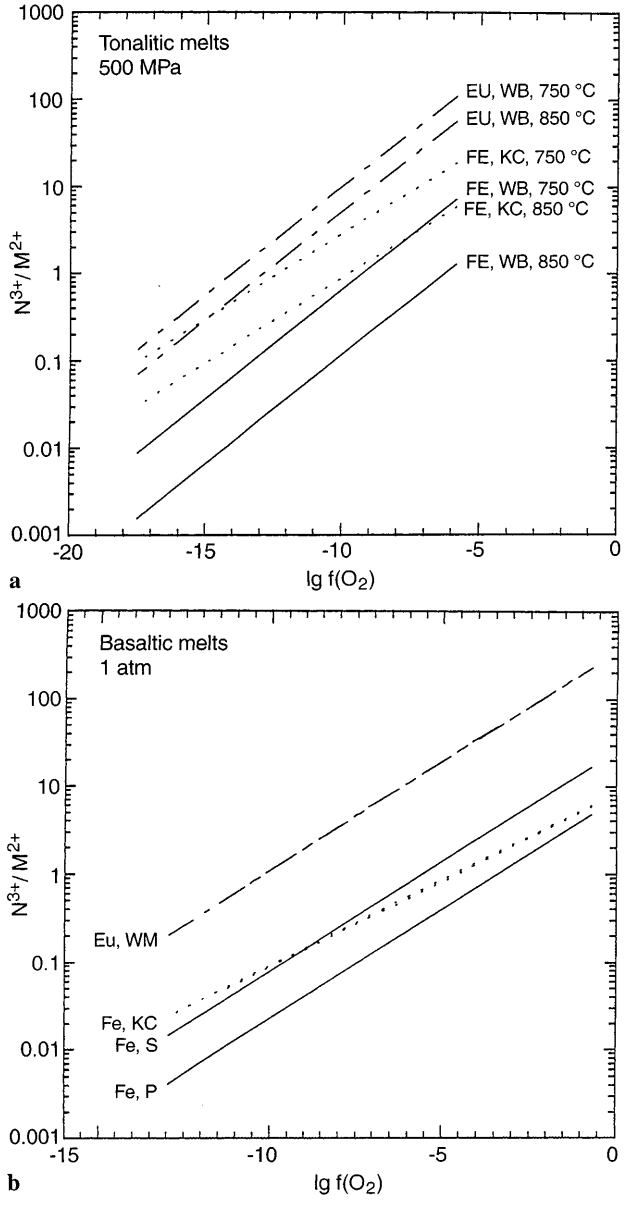

Fig. 6a M^{2+}/M^{3+} ratios versus log f_{O_2} for tonalitic melts at 500 MPa water pressure. Straight lines for Fe are calculated using the partitioning data (*WB*) and dotted lines using the empirical model of Kress and Carmichael (1991) (*KC*); *dashed-dotted lines* for Eu are calculated using partitioning data (*WB*). M^{2+}/M^{3+} ratios versus log f_{O_2} for basaltic melts at 1 atm. Straight lines are calculated using Fe partitioning data of Phinney (1992) (*P*) and Sato (1989) (*S*). Redox ratios of Fe calculated using the empirical model of Kress and Carmichael (1991) for the two datasets (*KC*, *dotted lines*) are virtually identical for both basaltic compositions. *Dashed-dotted lines* are calculated from Eu partitioning data of Weill and Mckay (1975) (*WM*)

$$\log f_{O_2} = 4 \cdot \log \frac{D_M - D_{M^{2+}}}{K_m \cdot (D_{M^{3+}} - D_M)} \quad . \tag{8}$$

In the case of tonalitic melts and temperatures between 750 and 850 °C the values of $D_{M^{2+}}$, $D_{M^{3+}}$ and K_m given in Table 3 may be directly used to calculate f_{O_2}. It is emphasised that the effect of temperature on Eu and Fe partitioning is small if oxygen fugacities relative to a buffer are considered ($\Delta NNO = \log(f_{O_2}/f_{O_2 NHO})$; $\Delta FMQ = \log(f_{O_2}/f_{O_2 FMQ})$) and thus an exact knowledge of the temperature in the magma chamber is not required. In contrast melt composition may have a strong influence on the partitioning parameters. For both Fe and Eu, K_m is dependent on the Al/Si ratio and degree of polymerisation of the melt (Mysen 1991; Moeller and Muecke 1984). Thus for application of the potential oxygen barometer to other magmatic systems K_m must be determined for the melts of interest (e.g. dacite or rhyodacite). $D_{M^{2+}}$ and $D_{M^{3+}}$ are dependant on the activities of the components involved in the exchange reactions. For instance, substitution of Eu^{2+} for Ca^{2+} in the plagioclase depends not only on the EuO activity in the melt but also the activities of CaO in the melt and in the plagioclase. Therefore, a more detailed knowledge on the influence of chemical parameters on $D_{M^{2+}}$, $D_{M^{3+}}$ and K_m is required to use of Fe and Eu partitioning as an independent oxygen barometer. However, in combination with other methods (experimental determination of phase equilibria, analysis of compositions of Fe-Ti oxides in natural samples), element partitioning can give further constraints on the development of oxygen fugacity during magma genesis.

Acknowledgements This work was supported by the DFG Schwerpunktprogramm on Element Distribution. We appreciate the technical assistance provided by O. Diedrich, W. Hurkurck and B. Aichinger. This manuscript benefited from valuable discussions with Y. Zhang and F. Holtz on an early version of this manuscript. We thank H. Keppler and the anonymous reviewer for their helpful comments.

References

Andersen DJ, Lindsley DH (1988) Internally consistent solution models for Fe-Mg-Mn-Ti oxides: Fe-Ti oxides. Am Mineral 73: 714–726

Baker LL, Rutherford MJ (1996) The effect of dissolved water on the oxidation state of silicic melts. Geochim Cosmochim Acta 60: 2179–2187

Behrens H (1995) Determination of water solubilities in high-viscosity melts: an experimental study on $NaAlSi_3O_8$ and $KAlSi_3O_8$ melts. Eur J Mineral 7: 905–920

Behrens H, Nowak M (1997) The mechanism of water diffusion in polymerized silicate melts. Contrib Mineral Petrol 126: 377–385

Behrens H, Johannes W, Schmalzried H (1990) On the mechanism of cation diffusion processes in ternary feldspars. Phys Chem Minerals 17: 62–78

Chou IM (1986) Permeability of precious metals to hydrogen at 2 kb total pressure and elevated temperatures. Am J Sci 286: 638–658

Coombs DS (1954) Ferriferrous orthoclase from Madagascar. Mineral Mag 30: 409–427

De Santis R, Breedveld GJF, Pausnitz JM (1974) Thermodynamic properties of aqueous gas mixtures at advanced pressures. Ind and Eng Chem Process Des Dev 13: 374–377

Drake MJ (1975) The oxidation state of europium as an indicator of oxygen fugacity. Geochim Cosmochim Acta 39: 55–64

Drake MJ, Weill DF (1975) Partitioning of Sr, Ba, Ca, Y, Eu^{2+}, Eu^{3+} and other REE between plagioclase feldspar and magmatic liquid: an experimental study. Geochim Cosmochim Acta 39: 689–712

Eugster HP, Wones DR (1962) Stability relations of the ferruginous biotite, annite. J Petrol 3: 82–125

Evans BW, Scaillet B (1997) The redox state of Pinatubo dacite and the ilmenite-hematite solvus. Am Mineral 82: 625–629

Flowers GC (1979) Correction of Holloway's (1977) Adaption of the modified Redlich-Kwong equation of state for calculation of fugacities of molecular species in supercritical fluids of geologic interest. Contrib Mineral Petrol 69: 315–318

Fudali RF (1965) Oxygen fugacities of basaltic and andesitic magmas. Geochim Cosmochim Acta 29: 1063–1075

Gaillard F, Scaillet B, Pichavant M (1998) Kinetics of iron oxidation-reduction in hydrous silicic melts. Terra Nova 10, Abstr. Suppl. 1: 17

Grams M, Behrens H (1996) Water solubility in tonalitic melts. Terra Nova 8, Abstr. Suppl. 1: 23

Grochau B (1996) Einfluß chemischer Parameter auf die Fe-Mg Verteilung zwischen Granat und Biotit. PhD thesis, University of Hannover

Hofmeister AM, Rossman GR (1984) Determination of Fe^{3+} and Fe^{2+} concentrations in feldspar by optical absorption and EPR spectroscopy. Phys Chem Minerals 11: 213–224

Holland T, Powell R (1991) A compensated-Redlich-Kwong (CORK) equation for volumes and fugacities of CO_2 and H_2O in the range 1 bar to 50 kbar and 100–1600 °C. Contr Mineral Petrol 121: 303–308

Kilinc A, Carmichael ISE, Rivers ML, Sack RO (1983) The ferric-ferrous ratio of natural silicate liquids equilibrated in air. Contrib Mineral Petrol 83: 136–140

Kimata M (1988) The crystal structure of non-stoichiometric Eu-anorthite: an explanation of the Eu-positive anomaly. Mineral Mag 52: 257–262

Krautheim J, Johannes W, Ziegenbein D (1992) COH-MIX—Ein Programm zur Berechnung von COH-Fluiden. Eur J Mineral 4: 158

Kress VC, Carmichael ISE (1991) The compressibility of silicate liquids containing Fe_2O_3 and the effect of composition, temperature, oxygen fugacity and pressure on their redox states. Contrib Mineral Petrol 108: 82–92

Lindsley DH, Frost BR (1992) Equilibria among Fe-Ti oxides pyroxenes, olivine and quartz: Part 1. Theory, Am Mineral 77: 987–1003

Linnen RJ, Pichavant M, Holtz F, Burgess S (1995) The effect of f_{O_2} on the solubility, diffusion and speciation of tin in haplogranitic melt at 850 °C and 2 kbar. Geochim Cosmochim Acta 59: 1579–1588

Longhi J, Walker D, Hays JF (1976) Fe and Mg in plagioclase. Proc Seventh Lunar Sci Conf: 1281–1300

Martel C, Pichavant M, Bourdier JL, Traineau H, Holtz F, Scaillet B (1998) Magma storage conditions and control of eruption regime in silicic volcanoes: experimental evidence from Mt. Pelée. Earth Planet Sci Letters 156: 89–99

Moeller P, Muecke GK (1984) Significance of europium anomalies in silicate melts and crystal-melt equilibria: a reavaluation. Contrib Mineral Petrol 87: 242–250

Moore G, Righter K, Carmichael ISE (1995) The effect of dissolved water on the oxidation state of iron in natural silicate liquids. Contrib Mineral Petrol 120: 170–179

Morris RV, Haskin LA, Biggar GM, O'Hara MJ (1974) Measurement of effects of temperature and partial pressure of oxygen on the oxidation states of europium in silicate glasses. Geochim Cosmochim Acta 38: 1447–1459

Mysen BO (1991) Relations between structure, redox equilibria of iron, and properties of magmatic liquids. In: Perchuk LL, Kushiro I (eds) Advances in physical chemistry vol. 9, pp 41–98

Mysen BO, Virgo D, Neumann ER, Seiffert FA (1985) Redox equilibria and the structural states of ferric and ferrous iron in melts in the system CaO-MgO-Al_2O_3-SiO_2-Fe-O: relationships between redox equilibria, melt structure and liquidus phase equilibria. Am Mineral 70: 317–331

Nowak M, Behrens H (1997) An experimental investigation on diffusion of water in haplogranitic melts. Contrib Mineral Petrol 126: 365–376

Phinney WC (1992) Partition coefficients for iron between plagioclase and basalt as a function of oxygen fugacity: implications for Archean and lunar anorthosites. Geochim Cosmochim Acta 56: 1885–1895

Popp RK, Nagy KL, Hajash A (1984) Semiquantitative control of hydrogen fugacity in rapid-quench hydrothermal vessels. Am Mineral 69: 557–562

Puziewicz J, Johannes W (1988) Phase equilibria and compositions of Fe-Mg-Al minerals and melts in water saturated peraluminous granitic systems. Contrib Mineral Petrol 100: 156–168

Robie RA, Hemingway BS (1995) Thermodynamic properties of minerals and related substances at 298.15 K and 1 bar (10^5 Pascals) pressure and at higher temperatures. US Geol Surv Bull 2131

Rutherford MJ, Devine JD (1996) Preeruption pressure-temperature conditions and volatiles in the 1991 dacitic magma of Mount Pinatubo. In Newhall CG, Punongbayan RS (eds) Fire and mud: eruptions and lahars of Mount Pinatubo, Philipinnes. PHIVOLCS and University of Washington Press, Seattle, pp 751–766

Sack RO, Carmichael ISE, Rivers M, Ghiorso MS (1980) Ferric-ferrous equilibria in natural silicate liquids at 1 bar. Contrib Mineral Petrol 75: 369–376

Sato H (1989) Mg-Fe partitioning between plagioclase and liquid in basalts of Hole 540B, ODP Leg 111: a study of melting at 1 atm. Proc Ocean Drill Prog Sci Res 11: 17–26

Scaillet B, Pichavant M, Roux J (1995) Experimental crystallization of leucogranite magmas. J Petrol 36: 663–705

Schmidt BC (1996) Conditions de fusion partielle et mecanismes d'incorporation de H_2 et H_2O dans les magmas haplogranitiques. PhD thesis, University of Orleans, France

Schulze F, Behrens H, Holtz F, Roux J, Johannes W (1996) The influence of water on the viscosity of a haplogranitic melt. Am Mineral 81: 1155–1165

Spencer KJ, Lindsley DH (1981) A solution model for coexisting iron. titanium oxides. Am Mineral 66: 1189–1201

Taylor JR, Wall VJ, Pownceby MI (1992) The calibration and application of accurate redox sensors. Am Mineral 77: 284–295

Truckenbrodt J, Ziegenbein D, Johannes W (1997) Redox conditions in piston-cylinder apparatus: the different behavior of boron nitride and unfired pyrophyllite assemblies. Am Mineral 82: 337–344

Weill DF, McKay GA (1975) The partitioning of Mg, Fe, Sr, De, Sm, Eu and Yb in lunar igneous systems and a possible origin of KREEP by equilibrium partital melting. Proc 6th Lunar Sci Conf: 1143–1158

Wilke M (1999) Partitioning of iron and europium between plagioclase and hydrous melt – a possible indicator for oxygen fugacities during igneous petrogenesis. PhD thesis, University of Hannover

Wilke M, Behrens H (1998) Ferric-ferrous ratios in tonalitic melts – the influence on iron partitioning between plagioclase and melt. Eur J Mineral 10: 318